RESEARCH PAPER

Comparative Therapeutic Efficacy of Mesenchymal Stem Cell–Derived Microvesicles and Pumpkin Seed Oil as Drug Delivery Strategies in Bleomycin-Induced Pulmonary Fibrosis

Menna Allah Alsayed Mohamed [1]*, Manal R. Abd El-Haleem [1], Amal Saeed AbdElazem El-Shal [2], Mohamed Ghazy Attia Hablas [1]

[1]Histology and Cell Biology Department, Faculty of Medicine, Suez University, Suez, Egypt
[2]Biochemistry Department, Faculty of Medicine, Zagazig University, Sharqia, Egypt

Corresponding author:
Email:ID: melsayed049@gmail.com

ABSTRACT

Background: Pumpkin seed oil (PSO) is a natural antioxidant with antifibrotic properties, while mesenchymal stem cell–derived microvesicles (MSC-MVs) promote tissue regeneration through bioactive signaling. This study aimed to improve therapeutic strategies for lung fibrosis by comparing the effects of PSO and MSC-MVs on bleomycin (BLM) -induced lung injury in rats to achieve better prognosis.

Methods: Thirty-five adult male albino rats were housed under standard conditions and ethically used to study BLM -induced lung fibrosis. The rats were divided into control and experimental groups to evaluate the therapeutic effects of PSO and MSC-MVs. Lung fibrosis was induced by BLM, followed by treatment with PSO or MSC-MVs. Lung tissues were collected after 14 days to assess histological and immunohistochemical changes.

Results: Quantitative and morphometric analyses demonstrated highly significant differences among the studied groups ($P<0.001$). BLM markedly increased serum malondialdehyde (MDA) and interleukin-6 (IL-6) levels, collagen fiber deposition, and alpha smooth muscle actin (α-SMA) expression, indicating severe inflammation and fibrosis with pronounced structural and ultrastructural lung damage. Treatment with PSO significantly reduced these parameters compared to the BLM group, though values remained higher than controls, reflecting partial protection. MSC-MVs produced the most pronounced therapeutic effect, significantly lowering MDA, IL-6, collagen deposition, and α-SMA expression to near-control levels and restoring lung architecture and ultrastructure.

Conclusions: BLM administration successfully induced marked pulmonary fibrosis, as evidenced by significant increases in collagen deposition, α-SMA immunoreactivity, and serum MDA and IL-6 levels compared with controls..

Keywords: *Microvesicles, Pumpkin Oil, Ameliorating Bleomycin, Lung Fibrosis, Albino Rats*

How to cite this article: Mohamed MA, Hablas MGA, El-shal ASA, Abd El-Haleem MR; Comparative Therapeutic Efficacy of Mesenchymal Stem Cell–Derived Microvesicles and Pumpkin Seed Oil as Drug Delivery Strategies in Bleomycin-Induced Pulmonary Fibrosis,..Int J Drug Deliv Technol. 2026;16(8s): 920-929; DOI: 10.25258/ijddt.16.8s.102
Source of support: Nil.
Conflict of interest: None

INTRODUCTION

Pulmonary fibrosis (PF) is a chronic, progressive, age-related interstitial lung disease (ILD) with a high morbidity and mortality rate [1]. The progression of PF results in pulmonary dysfunction and poor prognosis in patients with various illnesses of known and unknown origin [2].

Interstitial PF is described by changed cellular arrangement of alveolar region with unequal disposition of collagen, and pulmonary inflammation is well-thought-out the root cause of lung fibrosis [3].

Bleomycin (BLM) is a common fibrogenic agent, provoking an initial adult respiratory distress syndrome-like injury with subsequent strong fibroproliferative response, severe abnormalities of the alveolar surfactant system accompanied by epithelial metaplasia [4].

Pumpkin seed oil (PSO), as a dietary antioxidant, is a rich source of unsaturated fatty acids and antioxidants inclusive of vitamin E, tannins, linoleic acid, oleic acid and alkaloids. Moreover, its antifibrotic and antiparasitic properties against schistosoma mansoni infection have been documented [5].

The seeds have wide pharmacological activities such as anti-diabetic, antibacterial, antifungal, anti-inflammation and antioxidant effects. It can complement staples in food by supplying vitamins and indispensable minerals that may not be present in staple diets [6].

Microvesicles are extracellular vesicles that are derived from the plasma membrane of these cells and exocytosed

**Author for Correspondence:* melsayed049@gmail.com

into the extracellular environment. Microvesicles are non-nucleated double layer membrane-bound structures transferring bioactive components like membrane-derived receptors, proteins, lipids, carbohydrates, and genetic material including mRNA and microRNAs similar to the cells from which they are derived [7].

Microvesicles can carry messages through bioactive molecules including receptors, other proteins including cytokines, chemokines involved in cellular signaling and/or migration, nucleic acids, and lipids then transfer them to the target cells to modulate their functions and help in tissue regeneration [8].

The aim of this work was to contribute to improvement of available therapeutic methods of treatment of lung fibrosis for better prognosis by comparing the therapeutic role of PSO and mesenchymal stem cells microvesicles (MSC-MVs) on the rat's lung changes induced by BLM.

Recently, extracellular vesicles, particularly mesenchymal stem cell–derived microvesicles, have gained attention as innovative drug delivery vehicles capable of transferring bioactive molecules to target tissues. Unlike traditional pharmacological agents, microvesicles offer targeted delivery, reduced systemic toxicity, and enhanced therapeutic bioavailability. Therefore, this study aimed to compare the therapeutic efficiency of MSC-MVs and PSO as two distinct drug delivery approaches in the management of bleomycin-induced pulmonary fibrosis

Materials and Methods:

Animals

This experimental study was conducted on 35 adult healthy male albino rats (8 weeks old, weighing 180-200 grams) were utilized in this study. Animals were kept randomly (5 rat\group) in healthy plastic cages. The rats were housed at room temperature 12-hour light/dark cycles and was provided with food and water ad libitum throughout the experiment. Animals were kept under observation for about 4 days for adaptation before the start of the experiment. The experiment was carried out according to the committee's guidelines for Research and Ethical

Issues of Zagazig University, Egypt.

Organs: Lung of adult male albino rats.

Chemicals:

BLM vials (BLEOCIP 15, Cipla Pharmaceutical Company, India, and Mumbai).

PSO purchased from Elhawag Company for Natural oils and Cosmetics (Egypt) licensed under no. 159, 2,150 in 2009).

MSC-MVs. Mesenchymal stem cell–derived microvesicles were isolated from conditioned media of cultured MSCs at the Biochemistry Department, Kasr Al-Ainy Faculty of Medicine, Cairo University.

Alpha smooth muscle actin (αSMA). Interleukin 6 (IL 6). Malondialdhyde (MDA): (Biodiagnostic, Egypt).

Experimental design:

Thirty-five adult male albino rats were divided into seven groups, with at least five rats per group, to compare the histological and immunohistochemical effects of MSC-MVs and PSO on BLM -induced lung fibrosis. Group I (Control group) consisted of four subgroups: Subgroup IA (Negative control) with no treatment, Subgroup IB (Positive control) injected with 0.1 ml of phosphate-buffered saline (PBS), Subgroup IC (Positive control) treated with PSO (1 ml/kg) via oral gavage for 14 days, and Subgroup ID (Positive control) treated with 100 µg of MSC-MVs via intravenous injection. Group II (BLM group) was injected intratracheally with 5 IU/kg of BLM and sacrificed on day 14 [9]. Group III (BLM with PSO) was similarly treated with BLM, followed by PSO administration for 14 consecutive days [10]. Group IV (BLM with MVs-treated group) received BLM on day 1, followed by a single intravenous dose of MSC-MVs on day 2, and lung specimens were collected after 14 days. The study aimed to evaluate the effects of PSO and MSC-MVs on lung fibrosis induced by BLM.

Sample collection:

Rats were fasted overnight and anesthetized with 50 mg/kg sodium pentobarbital [11]. Two milliliters of blood were withdrawn via cardiac puncture and placed in vacutainers to clot. After 20 minutes, an incision was made, and both lungs were dissected, washed with saline, and divided into two specimens. One lung was fixed in 10% buffered formol saline for histological and immunohistochemical analysis, while the other was fixed in 2.5% glutaraldehyde for electron microscopy. Animal disposal followed safety and environmental protocols, with the carcasses sent for incineration at Zagazig Faculty of Medicine.

Preparation of micro vesicles (MVs):

MVs were isolated from MSCn conditioned medium. MSCs were cultured in DMEM for 24-48 hours, after which the medium was collected and centrifuged at 1000 rpm for 5 minutes and 2500 rpm for 15 minutes. The supernatant was filtered through a 0.45 µm filter to remove cellular debris. MVs were isolated by ultracentrifugation at 100,000 g for one hour at 4°C, and the pellets were resuspended in PBS and stored at -80°C [12]. Characterization included transmission electron microscopy (TEM) and flow cytometry for CD63 (extracellular vesicle marker) [13]. MVs were labeled with PKH26 dye, washed, and then used for lung tissue examination using a fluorescent microscope to trace the labeled cells [14, 15]. Appropriate dye-only controls were included to exclude false-positive PKH26 labelling.

Histological analysis:

Light microscope examination:

The tissue sections were processed for Hematoxylin and Eosin (H&E) staining by first deparaffinizing in xylene (10 minutes, three changes), followed by rehydration through descending alcohol grades (95%, 80%, 60%) for 1-2 minutes each. After rinsing in tap water, the sections were stained with Harris hematoxylin for 15 minutes, then differentiated in acid alcohol (1% HCl in 70% alcohol) for 5-10 seconds. The tissue was blued by washing in running tap water for 10-15 minutes and counterstained with eosin for 2-3 minutes. Dehydration followed in ascending alcohol grades, and the sections were cleared in xylene and mounted in Canada balsam. Masson’s Trichrome staining involved deparaffinization, rehydration, and rinsing in distilled water, followed by fixation in Bouin’s fixative [16]. The

sections were stained with Weigert's iron hematoxylin, blued, then stained sequentially with acid fuchsin, phosphomolybdic acid, and aniline blue. Differentiation was done with 2% acetic acid, and the sections were dehydrated, cleared in xylene, and mounted in a permanent medium. Both stains were examined and photographed under an Olympus light microscope in the Histology Department at Zagazig University.

Immunohistochemical staining:

Alpha-actin-2, also known as alpha smooth muscle actin (α-SMA), is a highly conserved protein involved in cell motility, structure, and contractility [17, 18]. It is a major component of the smooth muscle contractile apparatus and is commonly used as a marker for myofibroblast formation. The α-SMA antibody (Catalog Number: GB12045) recognizes human α-SMA and is suitable for applications like Western blot (WB), immunohistochemistry (IHC), and immunofluorescence (IF) in human, mouse, and rat tissues, including heart, liver, lung, colon, and brain. The antibody is affinity-purified, with a predicted and observed molecular weight of 42 kDa. It is stored at -20°C in PBS with 0.02% sodium azide and 50% glycerol. In IHC analysis, mouse lung tissue was processed with antigen retrieval, followed by primary antibody incubation overnight, and secondary antibody incubation for 1 hour. The resulting brown cytoplasmic/nuclear staining indicates α-SMA expression, with negative and positive control sections confirming the results.

Transmission electron microscope examination:

Transmission electron microscopy (TEM) creates detailed images using transmitted electrons. Specimens are fixed in 2.5% glutaraldehyde, post-fixed in osmium tetroxide, and washed. After dehydration through ethanol gradients, specimens are infiltrated with epoxy resin using acetone, then polymerized. Semi-thin (1 µm) sections are stained with toluidine blue and examined for areas suitable for ultrathin sectioning (75 nm). These sections are double-stained with uranyl acetate and lead citrate for enhanced contrast and viewed with a JEOL-JEM-100 SX electron microscope. Flow cytometry is also used to analyze MSCs in lung tissues from BLM-injected rats, detecting markers such as CD34, CD63, and CD29 [19, 20].

Estimation of Malondialdehyde (MDA) in tissue (lung) homogenate:

MDA was estimated by using Rat Malondialdehyde, MDA ELISA Kit supplied by (Biodiagnostic, Egypt). To perform the assay, allow all reagents to reach room temperature and mix thoroughly by gently swirling, avoiding foaming. Use only the required number of strips and store any extras at 4°C. Prepare all reagents, standards, and samples as directed. Add 50 µl of Standard, Blank, or Sample to each well, followed by 50 µl of Detection A working solution. Seal the plate and incubate for 1 hour at 37°C. Wash each well three times with Wash Buffer, then add 100 µl of Detection Reagent B and incubate for 45 minutes at 37°C. Wash five times, then add 90 µl of Substrate Solution and incubate for 15-30 minutes at 37°C, protecting from light. Add 50 µl of Stop Solution, ensuring uniform color change, then measure the optical density at 450 nm using a microplate reader.

Determination of inflammatory cytokines: Interleukin 6 (IL 6):

IL-6 was estimated by using Rat Quantikine®ELISA, Rat IL-6 Immunoassay [21]. To perform the assay, bring all reagents and samples to room temperature. It is recommended to assay all standards, controls, and samples in duplicate. Prepare reagents, standard dilutions, controls, and samples as instructed. Remove excess microplate strips and store them in the resealed foil pouch with the desiccant pack. Add 50 µL of Assay Diluent to each well, followed by 50 µL of standard, control, or sample, and gently mix by tapping the plate. Incubate for 2 hours at room temperature. After incubation, wash each well five times with Wash Buffer, ensuring complete removal of liquid. Add 100 µL of Rat IL-6 Conjugate to each well, cover, and incubate for 2 hours. Repeat the washing steps, then add 100 µL of Substrate Solution and incubate for 30 minutes, protecting from light. Add 100 µL of Stop Solution, mix gently, and read the optical density at 450 nm within 30 minutes using a microplate reader, with wavelength correction if available.

Morphometric study:

Ten different non-overlapping randomly chosen fields (x400) from different sections of each rat of each group were investigated to measure: Area percent of collagen. The area percent of αSMA positive cells. The total area was measured after selection by adjusting the color threshold while excluding the background; thereafter, the brown-stained area was selected and measured to calculate the area % as brown-stained area/total area × 100.

Statistical analysis:

The data obtained were statistically analyzed using SPSS software version 20 (SPSS Inc., Chicago, IL, USA), then compared by one-way analysis of variance (ANOVA) test followed by Tukey's test to compare different groups with the control group. The results were expressed as mean ± standard deviation (SD). The differences were considered statistically significant if the probability value ($P < 0.05$), highly significant if ($P < 0.001$), and non-significant if ($p > 0.05$) [22].

RESULTS:

Histological results:

Haematoxylin and eosin stain (H&E):

Control Group: The examined sections of all subgroups of the control group showed normal lung parenchyma with preserved architecture of bronchioles, alveolar sacs, alveoli and thin interalveolar septa. **(Figure 1, I and II)**

BLM-treated Group (II): Examination of H&E-stained sections of the lung revealed that, in many regions there is a progressive destruction of lung architecture. Areas of narrowing and collapse of alveolar space were observed. Thickening of interalveolar septa and walls of the blood vessels was also noticed. Obvious cellular infiltration was

detected in the interstitial tissue. The lungs of BLM-treated rats show congestion of the peri-alveolar and peri-bronchial blood capillaries, interstitial and intrabronchial hemorrhage. **(Figure 1, III, IV, V, VI)**

PSO Group (III): Examination of H&E-stained sections of the lung: Administration of PSO to BLM intoxicated rats induced protection of the lung tissue that was characterized by fewer numbers of inflammatory cells infiltration, mild edema and hemorrhages occupying the lung alveoli and inter-alveolar septa. **(Figure 1, VII, VIII)**

BLM with MV treated group (group IV): revealed that most of alveoli and interalveolar septa restore their normal architecture. However, few areas showed narrowing of some alveoli. Mild cellular infiltration of the interstitium was also observed. **(Figure 1, IX, X, XI, XII)**

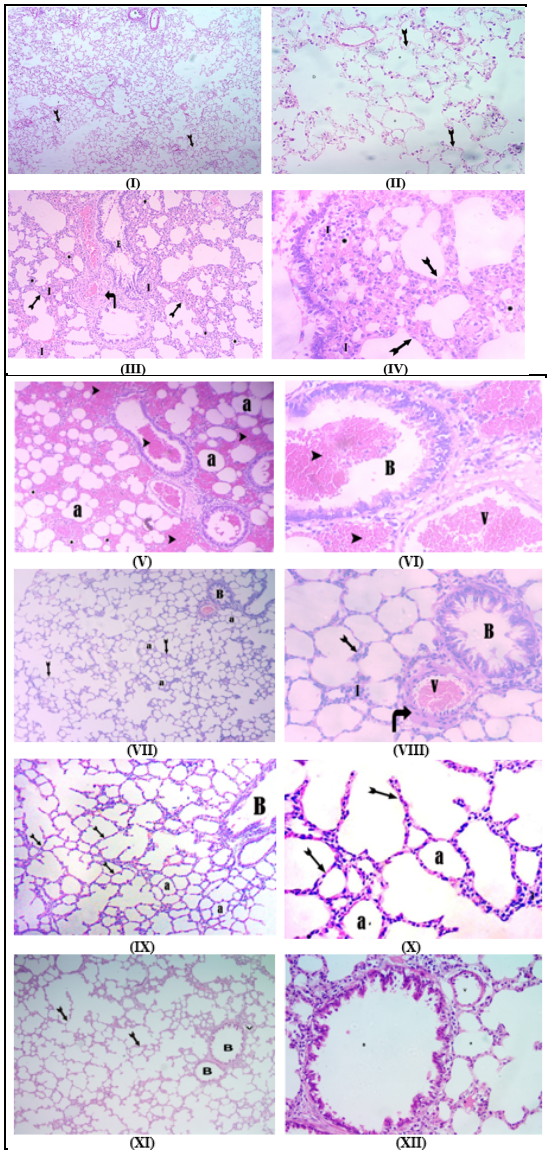

Figure 1: A photomicrograph of a section in the lung of Group I control group showing (I) normal lung: bronchiole (B), many alveoli (a) separated by thin interalveolar septa (arrows) (H&E, x100), (II) normal alveoli (a) with thin interalveolar septa (arrows) (H&E, x 400). Group II, (III) showing obvious destruction of the lung parenchyma, narrowing or even collapse (*) of alveolar spaces, detached bronchial epithelium (E), very thick interalveolar septa (arrows) Marked diffuse cellular infiltration (I) is also seen in the interstitium and congested blood vessel with thickened wall (curved arrow) (H&E, x100), (IV) markedly thickened interalveolar septa (arrows) with narrowing of the alveolar space (*). Obvious cellular infiltration (I) is also noticed(H&E, x 400), (V) obvious narrowing or even collapse of alveolar spaces (*). emphysematous alveoli also noticed (a) Marked interstitial hemorrhage and congestion (arrow heads) (H&E, x100), (VI) Marked interstitial hemorrhage and congestion (arrowheads), intrabronchial hemorrhage (B) and congested blood vessel (v) (H&E, x400). Group III showing (VII) nearly normal alveoli (a) most inter alveolar septa are thin with few thickened septa (arrows). Apparently normal bronchiole (B) (H&E, x100), (VIII) moderate thicking of the wall of blood vessel (curved arrow), congested vessel (v), a few thickened septa (arrows), a few cellular infiltrations (I) are also seen in the interstitium and apparently healthy bronchiole (H&E, x400). Group IV showing (IX) normal alveoli (a) with apparent thin interalveolar septa (arrows). A part of a bronchiole (B) appears nearly normal except for focal detachment of its epithelial lining (H&E, x100), (X) patent alveoli (a) with apparent thin alveolar walls (arrows) and mild cellular infiltration (I) in the interstitium and nearly normal bronchiole (H&E, x400), (XI) normal alveoli (a) with apparent thin interalveolar septa (arrows). a bronchiole (B) appears nearly normal (H&E, x100), (XII) patent alveoli (a) and mild cellular infiltration (I) in the interstitium and nearly normal bronchiole (H&E, x400)

Masson's Trichrome-stained sections results:

Control Group: revealed fine collagen fibers in the interalveolar septa, the adventitia of bronchioles and adventitia of blood vessels. **(Figure 2, A)**

BLM group (group II): showed obvious deposition of collagen fibers in the thickened interalveolar septa as well as in the adventitia of bronchioles and blood vessels. **(Figure 2, B)**

PSO Group (III): Masson's Trichrome-stained sections results: revealed scattered fine collagen fibers in the interalveolar septa, adventitia of the bronchioles and that of the blood vessels. **(Figure 2, C)**

BLM with MV treated group (group IV): There was a marked decrease of septal thickening with few inflammatory cells infiltration and marked reduction in collagen fiber deposition in the inter-alveolar septa.

(Figure 2, D)

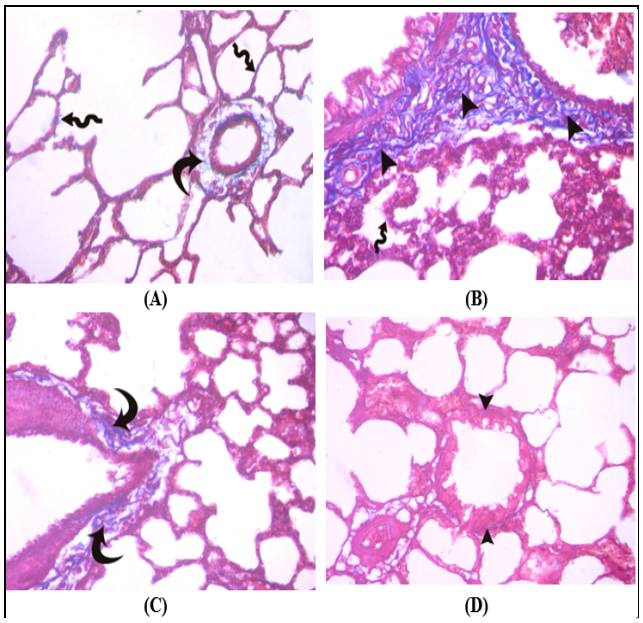

Figure 2: A photomicrograph of a section in the lung of Group I control group showing (A) Fine collagen fibers in the interalveolar septa (wavy arrows) and in the adventitia of an arteriole (curved arrow) are noticed. Group II, (B) Deposition of collagen fibers in the wall of a bronchiole (arrow heads) and arteriole. Collagen fibers in the thickened interalveolar septa (wavy arrow) are also detected. Group III (C)showing fine collagen fibers in the interalveolar septa (arrows), in the adventitia of an arteriole (curved arrow). Group IV, (D)fine collagen fibers around bronchiole (arrow heads) and in the adventitia of an arteriole (curved arrow) are noticed. (Masson's Trichrome, X400)

Immunohistochemical-stained sections result for α-SMA:

Control group (Group I): The lung sections examined showed no immunohistochemical reaction for α- SMA. **(Figure 3, A)** Sections of group I showed normal mild positive expression of α-SMA only around the blood vessels and in the sub-epithelial cells of the bronchioles. **(Figure 3, B)**

BLM group (group II): numerous cells with positive immunoreactivity for αSMA in the interalveolar septa. Positive immunoreactivity in the walls of blood vessels and bronchioles was also noticed showing strong expression of α-SMA within fibroblastic foci in the myofibroblast phenotype and variable types of cells; in the alveolar interstitium and some airway epithelial cells. **(Figure 3, C and D)**

PSO Group (III): showing decreased expression of α-SMA within the fibrotic interalveolar septa although scattered α-SMA immunopositive cells (arrow) among the proliferated cells in the interalveolar septa observed, compared to the BLM-treated lung. **(Figure 3, E)**

BLM with MV treated group (group IV): showing decreased thickening of the interalveolar septa with marked decrease in α- SMA immunopositive cells**.**

(Figure 3, F)

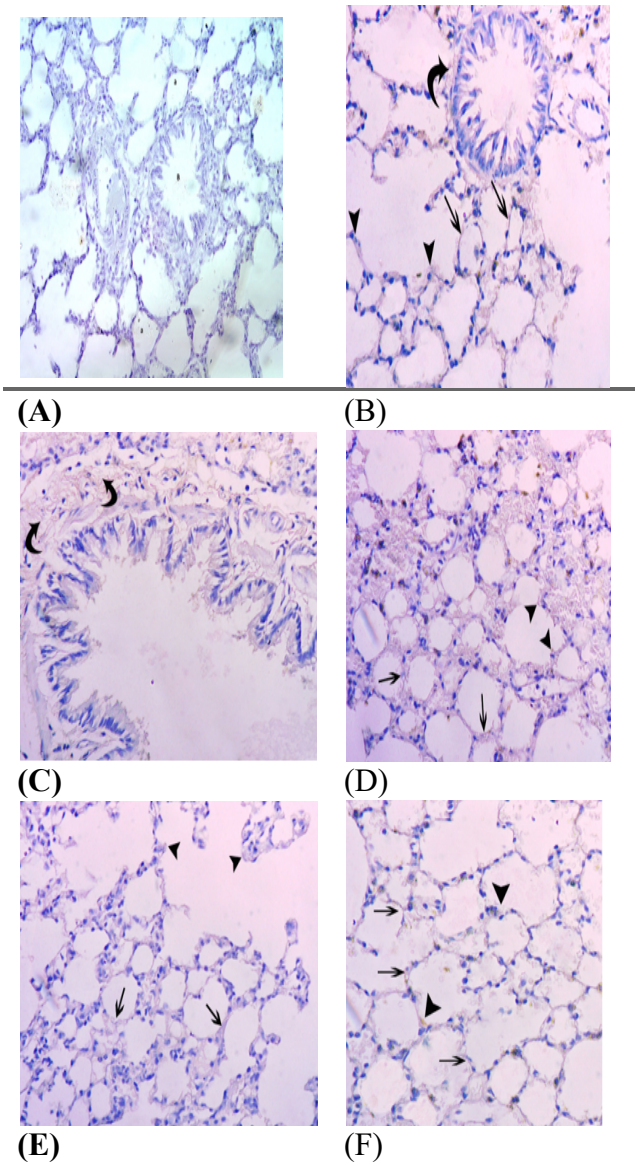

Figure 3: A photomicrograph of a section in the lung of Group I control group showing negative control section of the lung tissue showing (A) no immunohistochemical reaction for αSMA (αSMA immunostaining, x400), (B) positive reaction in the knobs of the alveolar ducts (arrowheads) and Positive reactions around bronchiole (curved arrow) can be detected. Few immunopositivity cells are seen in the alveolar wall (arrow) (αSMA immunostaining, x400). Group II, (C) Positive reactions around bronchiole (curved arrow) can be detected, (D) many cells exhibit positive immunoreactivity for αSMA in the interalveolar septa (arrows). positive reaction in the knobs of the alveolar ducts (arrowheads). Group III (E)showing fewer cells with moderate positive cytoplasmic immunoreaction in the interstitium and the interalveolar septa exhibit positive immunoreactivity for αSMA in the interalveolar septa (arrows). positive reaction in the knobs of the alveolar ducts (arrowheads). Group IV (F) showing few cells with positive immunoreactivity for αSMA in the interalveolar septa (arrows). Positive reaction in the knobs of the alveolar ducts (arrowheads). (αSMA immunostaining, x400).

Mean area % of collagen fiber deposition and α-SMA immune reaction in the lung in different studied groups:

The morphometric analysis showed a highly significant difference in collagen fiber deposition and α-SMA immune reaction between the four groups (P<0.001). In group II (BLM), the mean collagen deposition was significantly higher compared to groups I, III, and IV. Group III (BLM + PSO) had significantly reduced collagen deposition compared to group II, but higher than groups I and IV. Group IV (BLM with MVs) showed the lowest collagen deposition, significantly lower than both group II and III. Similarly, α-SMA immune reaction in group II was significantly higher than in groups I, III, and IV. Group III showed a significant decrease in α-SMA compared to group II, with a significant increase compared to groups I and IV. Group IV had the lowest α-SMA immune reaction, significantly lower than both group II and III. No significant differences were found within the subgroups of the control group (IA, IB, IC, ID) or between groups I and IV. **Table 1**

Table 1: The mean area % of collagen fiber deposition and α-SMA immune reaction in the lung in different studied groups using one-way ANOVA test followed by Tukey's test

		Collagen fiber deposition	TUKEY'S test	ANOVA	
				F	P
Group I	IA	3.57±0.235	2,3	12.396	<0.001 *
	IB	3.44±0.257	2,3		
	IC	3.47±0.270	2,3		
	ID	3.68±0.168	2,3		
Group II		15.61±0.429	1,3,4		
Group III		6.36±0.268	1,2,4		
Group IV		3.62±0.304	2,3		
α-SMA immune reaction					
Group I	IA	2.73±0.088	2,3	20.01	<0.001 *
	IB	2.74±0.060	2,3		
	IC	2.89±0.152	2,3		
	ID	2.75±0.151	2,3		
Group II		12.82±0.195	1,3,4		
Group III		5.36±0.313	1,2,4		
Group IV		2.87±0.227	2,3		

Data are presented as mean ± SD. *Significant P Value <0.05. 1: high sig. diff. from G(I), 2: high sig. diff. from G (II), 3: high sig. diff. from G (III), 4 highly sig. diff. from G (IV), α-SMA: anti α-smooth 13 muscle actin.

Electron Microscopic Results:

Control group (Group I): Ultrastructural examination of the control group showed type I pneumocyte that was flattened in shape with its flat nucleus filling most of the cytoplasm in addition to, normally appeared blood vessel with its lining endothelial cells. Furthermore, type II pneumocytes appeared as cuboidal shaped cells with euchromatic rounded nuclei. Their cytoplasm contained mitochondria, numerous lamellar bodies besides. thin interalveolar septum with normal blood capillary lined by endothelial cell nucleus. **(Figure 4, A, B, C)**

BLM group (group II): The examined ultrathin sections of the lung of group II showed changes in the alveolar lining cells. Moreover, type II pneumocytes showed nuclear membrane irregularities and nuclear indentation. Besides, apparently enlarged mitochondria. Type I pneumocytes appeared irregular with irregular nucleus. Regarding the lining endothelium of the blood vessels, irregular, shrunk nucleus with nuclear membrane irregularities were seen Moreover, there was extravasation of RBCs together with inflammatory cellular infiltrations, most probably eosinophils. thick interalveolar septum with infiltration by neutrophil. **(Figure 4, D, E, F, G, H)**

BLM with Pumpkin oil group (group III): The examined ultrathin sections of the lung of (group III) showed moderate improvement through which. Type II pneumocytes were found with nuclear indentation, abnormal shaped mitochondria, in addition to some empty lamellar bodies and an area of cytoplasmic rarefaction besides, scattered microvilli on their luminal surfaces, type I pneumocyte was seen with its flattened nucleus. The blood vessel was lined with abnormal endothelium with nuclear indentation.

(Figure 4, I, J)

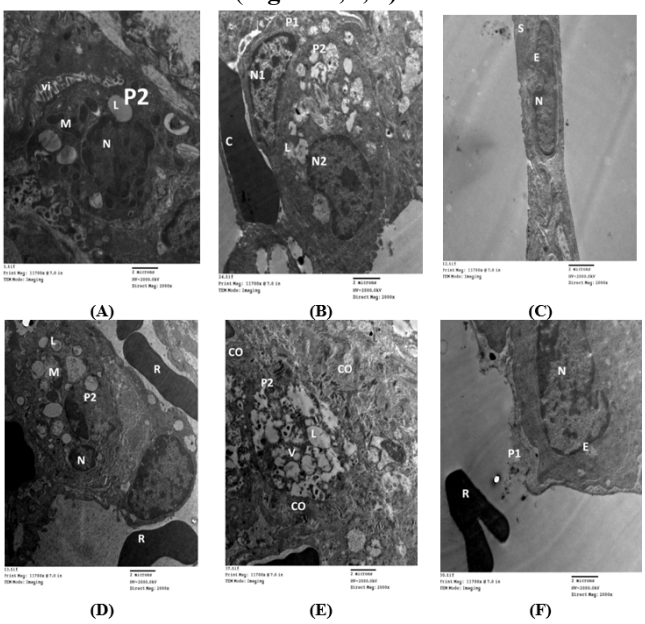

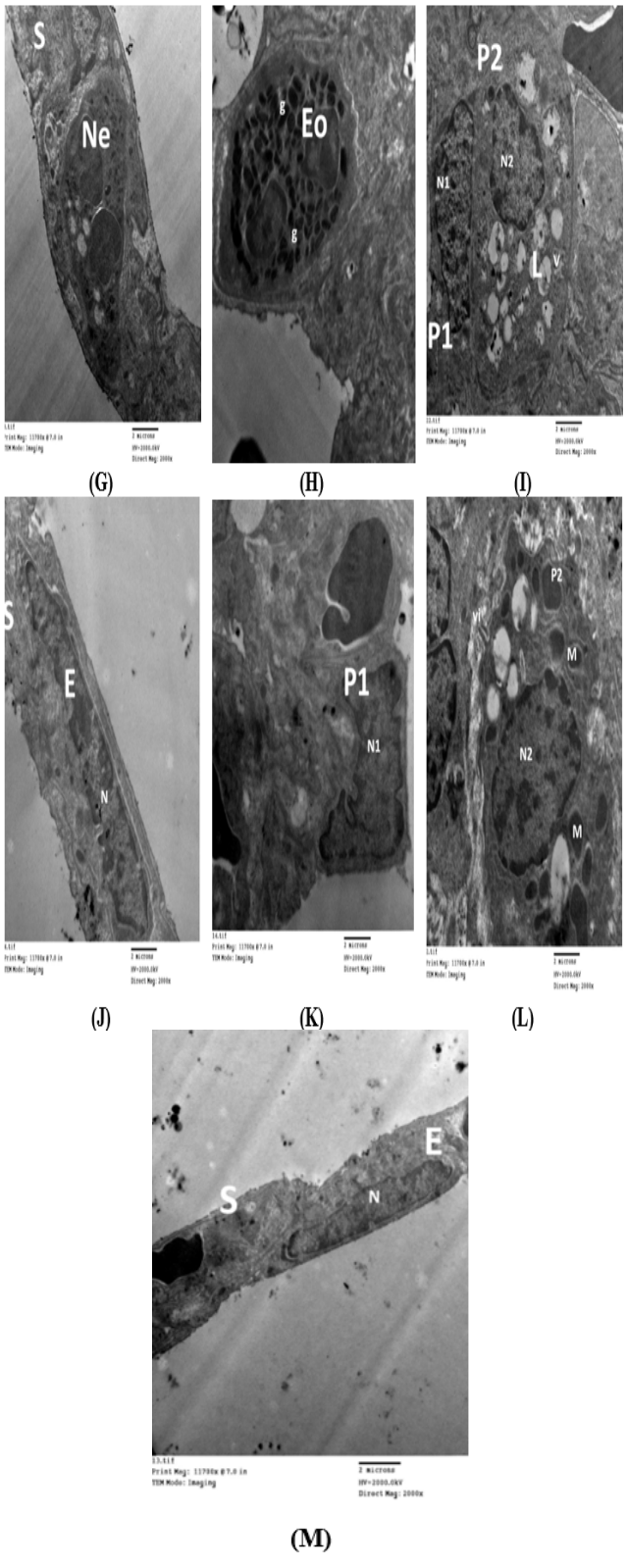

BLM with MV treated group (group IV): The examined ultrathin sections of the lung of (group IV) showed nearly normal lung ultrastructure. There was type I pneumocyte with its flattened nucleus. Also, type II pneumocyte appeared with its euchromatic rounded nucleus, mitochondria and refilled lamellar bodies. Furthermore, a nearly normal blood vessel with its lining endothelium was observed thin interalveolar septum. **(Figure 4, K, L, M)**

Figure 4: Electron micrograph of an ultrathin section of the lung from the control group showing (A) type II pneumocyte (P2) which is cuboidal in shape with an euchromatic rounded nucleus (N), mitochondria (M), numerous lamellar bodies (L), and short microvilli on its luminal surface (vi), (B) type II pneumocyte (P2) which is cuboidal in shape with an euchromatic rounded nucleus (N), mitochondria (M), numerous lamellar bodies (L), and short microvilli on its luminal surface (vi)(Mic. Mag. X2000), (C) thin interalveolar septum (s) with normal blood capillary lined by endothelial cell (E) nucleus (N), Electron micrograph of an ultrathin section of the lung from the bleomycin treated group II showing (D) type II pneumocyte (P2) with nuclear membrane irregularities and fragmented nucleus (N2). Notice: extravasation of RBCs (R), (E) type II pneumocyte (P2) many cytoplasmic vacuoles (V) and many collagen fibers surrounding it (Co), (F) irregular shaped fragmented type I pneumocyte (P1), thick blood barrier with irregular endothelial cell (E) nucleus (N)**.** Notice: extravasation of RBCs (R), (G) thick interalveolar septum (s) with infiltration by neutrophil (Ne), (H) interstitial infiltrations with eosinophils (Eo) with its characteristic granules (g), Electron micrograph of an ultrathin section of the lung BLM with Pumpkin oil group (group III) showing (I) Type II pneumocytes (P2) were found with nuclear indentation (N2), in addition to some empty lamellar bodies (L), and some cytoplasmic vacuolation (v). type I pneumocyte (P1) was seen with its flattened nucleus (N1), (J) moderately thick interalveolar septum (S), moderately thick blood barrier and the blood capillary lined with endothelial cell (E) with dentate nucleus (N), Electron micrograph of an ultrathin section of the lung from MV treated group (group IV) (K) type I pneumocyte (P1) with its flattened nucleus (N1), (L) type II pneumocyte (P2) appeared with its euchromatic rounded nucleus (N), mitochondria (M) and refilled lamellar bodies (L). It also contained microvilli on its luminal surface (vi), (M) thin interalveolar septum (s) with normal blood capillary lined by endothelial cell (E) nucleus (N) (Mic. Mag. X2000)

Biochemical results:

The quantitative analysis of the morphometric data revealed that the mean serum values of (MDA & IL-6) showed an overall highly significant difference between the four groups ($P<0.001$). Tukey's test analysis revealed that the mean levels of (MDA & IL-6) in group (II) were highly significantly increased compared to groups (I&III&IV). The mean levels of (MDA & IL-6) in groups (III) showed a highly significant decrease compared to group II while displayed a highly significant increase in this value versus groups (I& IV). The mean levels of (MDA & IL-6) in groups (IV) showed a highly significant decrease compared to (group II and group III). There was a non-significant difference between the subgroups of the control group (IA, IB, IC, ID). There was also no significant difference between groups (I & IV).

Table 2

Table 2: The mean serum values of MDA and of IL-6 in different studied groups using one-way ANOVA test followed by TUKEY'S test.

		MDA	TUKEY' S test	ANOVA	
				F	P-value
Group I	I A	0.67±0.089	2,3	10.81	<0.001 *
	I B	0.66±0.115	2,3		
	I C	0.62±0.104	2,3		
	I D	0.68±0.086	2,3		
Group II		13.86±0.859	1,3,4		
Group III		4.40±0.285	1,2,4		
Group IV		0.70±0.108	2,3		
		IL-6			
Group I	I A	135.06±4.15	2,3	18.53	<0.001 *
	I B	134.56±4.735	2,3		
	I C	131.69±4.816	2,3		
	I D	133.26±5.074	2,3		
Group II		561.82±6.570	1,3,4		
Group III		396.82±3.800	1,2,4		
Group IV		135.03±13.187	2,3		

Data are presented as mean ± SD. *Significant P Value <0.05. 1: highly sig. diff. from G(I), 2: highly sig. diff. from G (II), 3: highly sig. diff. from G (III), 4 highly sig. diff. from G (IV), α-SMA: anti α-smooth 13 muscle actin.

Discussion

Lung being one of the few internal organs that are exposed to a wide range of environmental pollutants including organic, inorganic and biological agents [23].

In the present research, Hematoxylin and Eosin-stained sections obtained from the BLM group showed changes in the lung parenchyma in the form of disorganized alveoli, alveolar collapse, significant increase in the thickness of the interalveolar septae, increase in the number of pneumocytes type II which proliferate at time of respiratory distress increasing surfactant secretion, Diffuse hemorrhagic area due to marked congestion and loss of elasticity in blood vessels, activation of myofibroblasts and increased collagen secretion leading to fibrosis and collapsed alveolar spaces. together with massive interstitial, and perivascular inflammatory cellular infiltrations. Our findings coincide with Hemmati et al. [24]; Elgendy et al. [25] found that there was significant decrease in alveolar spaces, thickening of the interalveolar septae and leukocytic infiltrations.

In the present study, Masson's trichrome staining of BLM group lung sections showed increased collagen fibers deposition around airways, blood vessels and in the interalveolar septa.

Histological evidence of lung injury such as thickening of alveolar walls, swelling and cellular infiltrates. The infiltrate was formed of different types of inflammatory cells but mostly composed of neutrophils, macrophages and eosinophils. The mean area % of collagen fiber deposition in groups III showed a highly significant decrease compared to group II while a highly significant increase in this value versus groups (I& IV). The mean area % of collagen fiber deposition in groups IV showed a highly significant decrease compared to group II and group III. This agreed with the results of El-mehi [5] illustrated that a significant reduction was observed in the area % of collagen deposition in the group treated with PSO group compared to diseased group. Likewise, Li et al. [26] explaining fibrosis by BLM induced epithelial injury.

Using α-SMA immunostaining, the lungs of the model group revealed many positively stained cells that were evident in the interalveolar septa in comparison to the little presence of such cells in the control group. The previous results were confirmed by that the mean area % of α-SMA immune reaction in groups III showed a highly significant decrease compared to group II while a highly significant increase in this value versus groups (I& IV). The mean area % of α-SMA immune reaction in groups IV showed a highly significant decrease compared to group II and group III. Supporting our study, Elgendy et al.[25] revealed that there was marked multifocal distortion of the lung architecture with significant increase of area % of α –SMA staining in BLM group compared to control group. These bodies are responsible for the ability of myofibroblasts to migrate, contract and apply traction on ECM. The level of expression of αSMA is proportionate to the level of activity of myofibroblasts

In this study, the biochemical analysis of MDA clarified that the mean levels of MDA in groups (III) showed a highly significant decrease compared to group II while displayed a highly significant increase in this value versus groups (I& IV). The mean levels of (MDA & IL-6) in groups (IV) showed a highly significant decrease compared to (group II and group III). Chen et al. [27] reported that oxidative stress affects cellular activity and aids in IPF progression. A two-way connection between oxidative stress and endoplasmic reticulum (ER) stress, a key factor in IPF, has been observed. This was supported by Abdelmoez [28] highlighted that the MDA levels were higher in the BLM group compared to the control group. In accordance to Albanawany et al. [29] these changes may be considered as an adaptation mechanism due to free radical exposures.

Examination of the lungs of group III (BLM with PSO group) showed marked reduction of numbers of inflammatory cells infiltration, mild edema and hemorrhages occupying the lung alveoli and inter-alveolar septa, moderate thickening of inter-alveolar septa. The mean levels of IL-6 in groups (III) showed a highly significant decrease compared to group II while displayed a highly significant increase in this value versus groups (I& IV). The mean levels of IL-6 in groups (IV) showed a highly significant decrease compared to (group II and group III). This aligned with Abdelmoez [28] highlighted that the IL-6 levels were higher in the BLM group compared to the

control group. Al-Okbi et al. [30] reported that PSO significantly inhibited the elevated plasma IL-6 and MDA levels, thereby reducing the severity of inflammation in arthritic rat model and producing significant improvements in inflammatory and oxidative stress biomarkers. Future studies should evaluate additional profibrotic mediators such as TGF-β.

MSCs have good anti- PF effects, but their applications are limited by their tumorigenicity and ethical considerations. MSC-MVs can avoid these challenges and are convenient for storage, which is conducive to large-scale production. MSC-MVs exhibited good anti- PF effects in BLM - induced PF rat models [23, 27].

The examined ultrathin sections of the lung (group IV) showed nearly normal lung ultrastructure. There was type I pneumocyte with its flattened nucleus. Also, type II pneumocyte appeared with its euchromatic rounded nucleus, mitochondria and refilled lamellar bodies. Furthermore, a nearly normal blood vessel with its lining endothelium was observed thin interalveolar septum.

Conclusions:

BLM administration successfully induced marked PF, as evidenced by significant increases in collagen deposition, α-SMA immunoreactivity, and serum MDA and IL-6 levels compared with controls. Treatment with PSO significantly attenuated these fibrotic, myofibroblastic, and inflammatory changes, although values remained higher than controls. These findings indicate that both interventions mitigate BLM-induced lung injury, with MSC-MVs demonstrating superior anti-fibrotic and anti-inflammatory efficacy. However, translation to human therapy requires further preclinical and clinical validation

Financial support and sponsorship: Nil

Conflict of Interest: Nil

REFERENCE

1. Diaz CM, Caballeria E, Torres JS. Comparative analysis of idiopathic pulmonary fibrosis and progressive pulmonary fibrosis: Epidemiology, pathophysiology, clinical features, diagnosis and treatment. Fibrosis. 2025;3:100-21.
2. Wang J, Li K, Hao D, Li X, Zhu Y, Yu H, et al. Pulmonary fibrosis: pathogenesis and therapeutic strategies. MedComm (2020). 2024;5:744-59.
3. Wang JY, Young LR. Insights into the pathogenesis of pulmonary fibrosis from genetic diseases. Am J Respir Cell Mol Biol. 2022;67:20-35.
4. Mohammed SM, Al-Saedi HFS, Mohammed AQ, Amir AA, Radi UK, Sattar R, et al. Mechanisms of bleomycin-induced lung fibrosis: A review of therapeutic targets and approaches. Cell Biochem Biophys. 2024;82:1845-70.
5. El-mehi AE-s. Effect of pumpkin seed oil on experimentally induced early liver fibrosis in the adult male albino rat. Egypt J Histol. 2023;46:796-809.
6. Grajzer M, Kozłowska W, Zalewski I, Matkowski A, Wiland-Szymańska J, Rękoś M, et al. Nutraceutical prospects of pumpkin seeds: A study on the lipid fraction composition and oxidative stability across eleven varieties. Foods. 2025;14:354-62.
7. Jurj A, Zanoaga O, Braicu C, Lazar V, Tomuleasa C, Irimie A, et al. A comprehensive picture of extracellular vesicles and their contents. Molecular transfer to cancer cells. Cancers. 2020;12:298-305.
8. Abbas A, Almaghrbi H, Giordo R, Zayed H, Pintus G. Pathogenic mechanisms, diagnostic, and therapeutic potential of microvesicles in diabetes and its complications. Arch Biochem Biophys. 2024;761:110-68.
9. Lai L, Zhou X, Chen H, Luo Y, Sui W, Zhang J, et al. Composition and diversity analysis of the B-cell receptor immunoglobulin heavy chain complementarity-determining region 3 repertoire in patients with acute rejection after kidney transplantation using high-throughput sequencing. Exp Ther Med 2019;17:2206-20.
10. Fawzy EI, El Makawy AI, El-Bamby MM, Elhamalawy HO. Improved effect of pumpkin seed oil against the bisphenol-A adverse effects in male mice. Toxicol Rep. 2018;5:857-63.
11. Ghasi S, Umana I, Ogbonna A, Nwokike M, Ufelle S. Cardioprotective effects of animal grade piperazine citrate on isoproterenol induced myocardial infarction in wistar rats: Biochemical and histopathological evaluation. Afr J Pharm Pharmacol. 2020;14:285-93.
12. Tang XD, Shi L, Monsel A, Li XY, Zhu HL, Zhu YG, et al. Mesenchymal stem cell microvesicles attenuate acute lung injury in mice partly mediated by Ang-1 mRNA. Stem Cells. 2017;35:1849-59.
13. Ali Moussa HY, Manaph N, Ali G, Maacha S, Shin KC, Ltaief SM, et al. Single extracellular vesicle analysis using flow cytometry for neurological disorder biomarkers. Front Integr Neurosci. 2022;16:879-82.
14. Dominkuš PP, Stenovec M, Sitar S, Lasič E, Zorec R, Plemenitaš A, et al. PKH26 labeling of extracellular vesicles: Characterization and cellular internalization of contaminating PKH26 nanoparticles. Biochim Biophys Acta. 2018;1860:1350-61.
15. Li X, Zhang Y, Yeung SC, Liang Y, Liang X, Ding Y, et al. Mitochondrial transfer of induced pluripotent stem cell–derived mesenchymal stem cells to airway epithelial cells attenuates cigarette smoke–induced damage. Am J Respir Cell Mol Biol 2014;51:455-65.
16. Leonard AK, Loughran EA, Klymenko Y, Liu Y, Kim O, Asem M, et al. Methods for the visualization and analysis of extracellular matrix protein structure and degradation. Methods in cell biology. 143: Elsevier; 2018. p. 79-95.
17. Afza F, Khan MA, Sharif M, Rehman A. Microscopic skin laceration segmentation and classification: A framework of statistical normal distribution and optimal feature selection. Microsc Res Tech. 2019;82:1471-88.

18. Cheville NF. Ultrastructural pathology: the comparative cellular basis of disease: John Wiley & Sons; 2009.
19. McKinnon KM. Flow Cytometry: An Overview. Curr Protoc Immunol. 2018;120:511-24.
20. Sober SA, Darmani H, Alhattab D, Awidi A. Flow cytometric characterization of cell surface markers to differentiate between fibroblasts and mesenchymal stem cells of different origin. Arch Med Sci. 2021;19:1487-95.
21. Hamza RZ, Al-Salmi FA, El-Shenawy NS. Chitosan and lecithin ameliorate osteoarthritis symptoms induced by monoiodoacetate in a rat model. Molecules. 2020;25:5738-48.
22. Stehlik-Barry K, Babinec AJ. Data analysis with IBM SPSS statistics: Packt Publishing Ltd; 2017.
23. Hu Y, Ciminieri C, Hu Q, Lehmann M, Königshoff M, Gosens R. WNT Signalling in Lung Physiology and Pathology. Handb Exp Pharmacol. 2021;269:305-36.
24. Hemmati AA, Pashmforosh M, Tabandeh MR, Rezaie A, RAJABI VH, Pipelzadeh MH, et al. Protective effects of morin against bleomycin-induced pulmonary fibrosis in mice. 2019.
25. Elgendy MS, Elsayed A, Eldosokey DE, Abd Elmaqsoud AK. Histological and immunohistochemical study to evaluate the effects of metformin versus green tea extracts on bleomycin induced lung injury in adult male albino rats. Egyptian Journal of Histology. 2021;44:31-47.
26. Li S, Shi J, Tang H. Animal models of drug-induced pulmonary fibrosis: an overview of molecular mechanisms and characteristics. Cell Biology and Toxicology. 2022;38:699-723.
27. Chen B, Hamdy H, Zhang X, Cao P, Fu Y, Shen J. From Fibrosis to Malignancy: Mechanistic Intersections Driving Lung Cancer Progression. Cancers. 2025;17:3861.
28. abdelmoez wa. Possible Protective Role of Pirfenidone Versus Combined Antifibrotic Therapy Colchicine and Pirfenidone in a Rat Model of Bleomycin Induced Pulmonary Fibrosis and Evaluation of their Potential Impact on α-SMA, IL6 and TGFβ (Histological and Immunohistochemical Study). Egyptian Journal of Histology. 2024;47:238-52.
29. Albanawany NM, Samy DM, Zahran N, El-Moslemany RM, Elsawy SM, Abou Nazel MW. Histopathological, physiological and biochemical assessment of resveratrol nanocapsules efficacy in bleomycin-induced acute and chronic lung injury in rats. Drug Deliv. 2022;29:2592-608.
30. Al-Okbi S, Mohamed DA, Kandil E, Abo-Zeid M, Mohammed S, Ahmed E. Anti-inflammatory activity of two varieties of pumpkin seed oil in an adjuvant arthritis model in rats. Grasas y Aceites. 2017;68:180-5.